Journal of Information & Optimization Sciences
ISSN 0252-2667 (Print), ISSN 2169-0103 (Online)
Vol. 46 (2025), No. 5, pp. 1479–1503
DOI : 10.47974/JIOS-1608

Response of memory to the imperfect fluid–double porous non–local thermoelastic solid interface

Rajesh Kumar ‡
Department of Mathematics
Indira Gandhi University
Meerpur 122502
Haryana
India

Vipin Gupta †
Department of Mathematics
Gurugram University
Gurugram 122003
Haryana
India

Vijayata Pathania §
Department of Mathematics
Himachal Pradesh University
Regional Center Dharamshala
Dharamshala 176057
Himachal Pradesh
India

M. S. Barak *
Department of Mathematics
Indira Gandhi University
Meerpur 122502
Haryana
India

‡ *ORCID-ID:* 0000-0003-2065-1372
† *ORCID-ID:* 0000-0002-5238-1963
§ *ORCID-ID:* 0000-0003-3842-0759
* *ORCID-ID:* 0000-0001-9947-000X

‡ *E-mail:* sangwan.rajesh33@gmail.com
† *E-mail:* vipin@gurugramuniversity.ac.in
§ *E-mail:* vpmsmrc@gmail.com
* *E-mail:* ms_barak@igu.ac.in (Corresponding Author)

Abstract

This manuscript delves into the study of plane wave behavior in a half-space denoted as M_1, representing a double porous nonlocal thermoelastic solid. This solid encompasses dual-phase-lag (DPL) effects with memory, interacting with an inviscid fluid half-space referred to as M_2. The model is solved using the eigenmode method after converting the dimensionless governing equations into a two-dimensional format. Through this investigation, it has been discerned that the medium M_1 exhibits five distinct types of waves: four longitudinal waves, one transverse wave, and one mechanical wave in M_2. By imposing boundary conditions at the interface, the corresponding secular equations are derived. The components of various physical fields are then obtained in closed form. Numerical simulations are employed to visualize the impact of nonlocal, memory, and stiffness on the fundamental properties of waves. Graphical representations effectively convey the outcomes of these simulations, providing insights into how these parameters influence wave characteristics.

Subject Classification: *74H45, 74J05, 74F05, 76S05.*

Keywords: *Non-local, Phase lags, Memory dependent derivatives, Double porosity, Stiffness.*

1. Introduction

The classical thermoelasticity theory does not explain the process driving thermal signal velocity. In classical thermoelasticity theory, thermal disturbances are expected to spread infinitely, which is unrealistic. Paradigm of nonlocal thermoelasticity, initially introduced by Edelen and Laws [1] and further refined by Eringen and Edelen [2], emerged as a groundbreaking departure from conventional thermoelastic approaches. In this theoretical framework, the constitutive variables' values are intricately linked to the overall system's characteristics, accounting for diverse physical parameters and specific site conditions such as mass, entropy, body force, and internal energy. Expanding upon this concept, Polizzotto [3] and Chakraborty [4] extended nonlocality to elasticity and various domains beyond. Exploring the ramifications of size-dependent thermal features in nano-scale heat transport, Kumar et al. [5] pioneered a nonlocal DPL model.

The word "memory-dependent derivative (MDD)", coined by Wang and Li [6], involves transforming the Caputo-type [7] derivative into an integral representation. The first order $(\alpha = 1)$ for time delay $\tau > 0$ of function *f* can be defined in an interval $[(t-\tau), t]$, with kernel $K(t-\zeta)$:

$$D_\tau f(t) = \frac{1}{\tau}\int_{t-\tau}^{t} K(t-\zeta) f'(\zeta) d\zeta. \tag{1.1}$$

Depending on the inherent characteristics of the given circumstance, the kernel function may be

$$K(t-\zeta)=1-\frac{2n}{\tau}(t-\zeta)+\frac{m^2}{\tau^2}(t-\zeta)^2=\begin{cases}1 & \text{if } n=m=0\\ 1-(t-\zeta)/\tau & \text{if } n=1/2, m=0\\ (1-(t-\zeta)/\tau)^2 & \text{if } n=m=1\end{cases} \quad (1.2)$$

Investigating the waves in thermoelastic double-porous materials carries significant significance across diverse domains, such as geomechanics, hydrogeology, and petroleum engineering. This significance arises from the fact that the majority of Earth's materials exhibit a combination of porosity and elasticity. Nunziato and Cowin [8] altered the conventional elasticity theory by specifically concentrating on integrating voids within elastic materials. Iesan [9] proposed a theoretical framework for thermoelastic solids containing voids and presented several theorems pertaining to the uniqueness of the solution. Iesan and Quintanilla [10] give the theoretical framework for thermoelastic materials with double porous architectures, incorporating nonlinearity. Barak, along with a dedicated team of researchers [11]–[18], delves into an extensive inquiry, meticulously investigating the profound implications of nonlocality and memory effects on the intricate phenomena of wave propagation across diverse media.

This study systematically explores the repercussions of MMD, stiffness, and nonlocal effects on wave propagation within an isotropic nonlocal homogeneous thermoelastic dual-phase lag half-space, denoted as M_1, juxtaposed with an inviscid fluid half-space M_2. Employing the eigenmode analysis, the study methodically formulates expressions for the pertinent variables, subsequently deriving a compact form of the secular equation by integrating thermal and mechanical boundary conditions. The investigation culminates in a detailed graphical representation of computer-simulated outcomes, exemplified through a material reminiscent of magnesium crystals. This meticulous examination advances our comprehension of wave dynamics within the specified thermomechanical context, contributing valuable insights into the intricate interplay of memory-dependent derivatives, stiffness, and nonlocality on the fundamental characteristics of wave propagation.

2. Field equations

After Eringen's work [19], the studies by Iesan and Quintanilla [10] and Ezzat et al. [20] guide us to the constitutive relation of a dual type of voids in the nonlocal thermoelastic medium that is isotropic and homogeneous. This material incorporates dual-phase-lag with MDD, considering the absence of external body force.

$$(1-\xi^2\nabla^2)\sigma_{ij}=\sigma_{ij}^L=\lambda\delta_{ij}e_{kk}+2\mu e_{ij}+b\delta_{ij}\psi-\beta_{ij}T \tag{2.1}$$

$$(1-\xi^2\nabla^2)\sigma_i^1=(\sigma_i^1)^L=a\phi_{,i}+b_1\psi_{,i} \tag{2.2}$$

$$(1-\xi^2\nabla^2)\sigma_i^2=(\sigma_i^2)^L=b_1\phi_{,i}+\gamma\psi_{,i} \tag{2.3}$$

$$(1-\xi^2\nabla^2)\zeta_1=(\zeta_1)^L=-be_{jj}-a_1\phi-a_3\psi+\gamma_1 T \tag{2.4}$$

$$(1-\xi^2\nabla^2)\zeta_2=(\zeta_2)^L=-de_{jj}-a_3\phi-a_2\psi+\gamma_2 T \tag{2.5}$$

The equations of motion:

$$\sigma_{ji,j}^L=\rho(1-\xi^2\nabla^2)\ddot{u}_i \tag{2.6}$$

$$(\sigma_{j,j}^1)^L+(\zeta_1)^L=\chi_1(1-\xi^2\nabla^2)\ddot{\phi} \tag{2.7}$$

$$(\sigma_{j,j}^2)^L+(\zeta_2)^L=\chi_2(1-\xi^2\nabla^2)\ddot{\psi} \tag{2.8}$$

The heat equation:

$$K(1+\tau_T D_{\tau_T})T_{,ii}=\left(1-\xi^2\nabla^2+D_{\tau_q}+a_0\frac{\tau_q^2}{2}D_{\tau_q}^2\right)(\beta T_0\dot{e}_{kk}+\gamma_1 T_0\dot{\phi}+\gamma_2 T_0\dot{\psi}+\rho C_e\dot{T}) \tag{2.9}$$

where, σ_i^1 and σ_i^2 are the equilibrated stress tensor, λ,μ indicate the Lame's constants, u_i denotes the component of displacement, the intrinsic equilibrated body forces is denoted by ζ_1 and ζ_2, b and d are voids parameters, ϕ and ψ are the volume fraction field of dual voids, ρ is the density, ∇ is the nabla operator, $\beta=(3\lambda+2\mu)\alpha_t$ is temperature coefficient, corresponding to thermal properties γ_1 and γ_2 are the constitutive coefficients, α_t is linear thermal expansion, a, a_1, a_2, a_3, b_1, γ represents the material constants, for type-I, II voids, χ_1 and χ_2 are the inertia coefficients, ξ is nonlocal parameter, T is the change in temperature,

C_e is the specific heat, K is the thermal conductivity, T_0 denotes the ambient temperature, τ_q & τ_T are the phase lags. Subscript L stands for local effect.

3. Problem formulation

We examine a semi-infinite nonlocal thermoelastic solid medium (M_1) containing dual types of voids, positioned beneath a semi-infinite inviscid fluid medium (M_2). The disturbance is confined to the neighborhood of $z=0$. The state variable is dependent on time t and x, z coordinates. The medium's displacement is denoted as $u_x = u(x,z,t)$, $u_z = w(x,z,t)$.

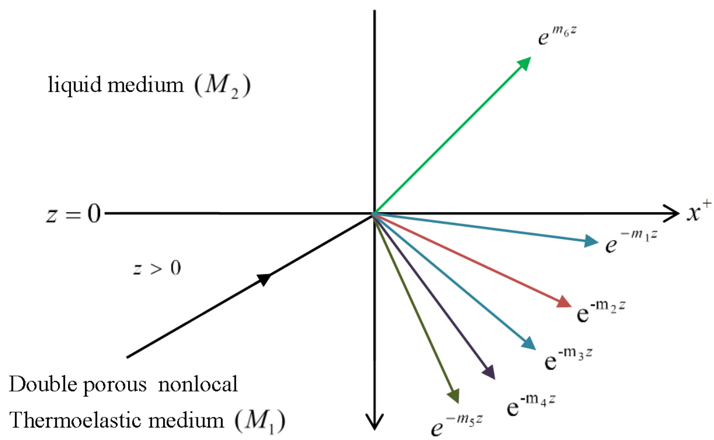

Figure 1

Schematic diagram of the problem

The equation of motions and equation of energy has been obtained by using the governing equations (2.1)-(2.9) in two-dimensional form as follows

$$(\lambda+2\mu)u_{,xx}+\mu(u_{,zz}+w_{,xz})+\lambda w_{,xz}+d\psi_{,x}+b\phi_{,x}-\beta T_{,x}=\rho(1-\xi^2\nabla^2)\ddot{u} \qquad (3.1)$$

$$(\lambda+\mu)u_{,xz}+\mu w_{,xx}+(\lambda+2\mu)w_{,zz}+d\psi_{,z}+b\phi_{,z}-\beta T_{,z}=\rho(1-\xi^2\nabla^2)\ddot{w} \qquad (3.2)$$

$$-b(u_{,x}+w_{,z})-a_1\phi+b_1(\psi_{,xx}+\psi_{,zz})+a(\phi_{,xx}+\phi_{,zz})-a_3\psi+\gamma_1 T=\chi_1(1-\xi^2\nabla^2)\ddot{\phi} \qquad (3.3)$$

$$-d(u_{,x}+w_{,z})-a_3\phi+\gamma(\psi_{,xx}+\psi_{,zz})+b_1(\phi_{,xx}+\phi_{,zz})-a_2\psi+\gamma_2 T=\chi_2(1-\xi^2\nabla^2)\ddot{\psi} \quad (3.4)$$

$$K(1+\tau_T D_{\tau_T})(T_{,xx}+T_{,zz})=\left(1-\xi^2\nabla^2+\tau_q D_{\tau_q}+a_0\frac{\tau_q^2}{2}D_{\tau_q}^2\right)\beta T_0(\dot{u}_{,x}+\dot{w}_{,x})+(\gamma_1 T_0\dot{\phi}+\gamma_2 T_0\dot{\psi}+\rho C_e\dot{T}) \quad (3.5)$$

Dimensionless formulas:

$$(x',z')=\frac{\omega_1}{c_1}(x,z),\ p_f'=\frac{1}{\beta T_0}p_f,\ (\phi',\psi')=\frac{\omega_1^2\chi_1}{c_1^2}(\phi,\psi),\ (u_f',w_f')=\frac{1}{c_1}(u_f,w_f),$$
$$(\sigma_{zz}',\sigma_{zx}')=\frac{1}{\beta T_0}(\sigma_{zz},\sigma_{zx}),\ (t',\tau'_T,\tau'_q)=\omega_1(t,\tau_T,\tau_q),\ (u',w')=\frac{\rho\omega_1 c_1}{\beta T_0}(u,w),$$
$$T'=\frac{T}{T_0},\ \xi'=\frac{\omega_1}{c_1}\xi,\ \phi_f'=\frac{\omega_1}{c_1^2}\phi_f \quad (3.6)$$

Equation (3.6) has been inserted into equations (3.1)-(3.5); the governing equations in their dimensionless form are presented as follows.

$$u_{,xx}+\delta^2 u_{,zz}+(1-\delta^2)w_{,xz}+f_2\psi_{,x}+f_1\phi_{,x}-T_{,x}=(1-\xi^2\nabla^2)\ddot{u} \quad (3.7)$$

$$(1-\delta^2)u_{,xz}+\delta^2 w_{,xx}+w_{,zz}+f_1\phi_{,z}+f_2\psi_{,z}-T_{,z}=(1-\xi^2\nabla^2)\ddot{w} \quad (3.8)$$

$$-f_4(u_{,x}+w_{,z})-f_5\phi+\phi_{,xx}+\phi_{,zz}+f_3(\psi_{,xx}+\psi_{,zz})-f_6\psi+f_7 T=\frac{1}{\delta_1^2}(1-\xi^2\nabla^2)\ddot{\phi} \quad (3.9)$$

$$-f_9(u_{,x}+w_{,z})+\phi_{,xx}+\phi_{,zz}-f_{10}\phi+f_8(\psi_{,xx}+\psi_{,zz})-f_{11}\psi+f_{12}T=\frac{1}{\delta_2^2}(1-\xi^2\nabla^2)\ddot{\psi} \quad (3.10)$$

$$(1+\tau_T D_{\tau_T})(T_{,xx}+T_{,zz})=\left(1-\xi^2\nabla^2+\tau_q D_{\tau_q}+a_0\frac{\tau_q^2}{2}D_{\tau_q}^2\right)(\varepsilon(\dot{u}_{,x}+\dot{w}_{,z})+f_{13}\dot{\phi}+f_{14}\dot{\psi}+\dot{T}) \quad (3.11)$$

where,

$$f_1=\frac{bc_1^2}{\omega_1^2\chi_1\beta T_0},\ f_2=\frac{dc_1^2}{\omega_1^2\chi_1\beta T_0},\ f_3=\frac{b_1}{a},\ f_4=\frac{\beta T_0\chi_1 b}{\rho c_1^2 a},\ f_5=\frac{a_1c_1^2}{a\omega_1^2},\ f_6=\frac{a_3c_1^2}{a\omega_1^2},$$

$$f_7=\frac{\gamma_1T_0\chi_1}{a},\ f_8=\frac{\gamma}{b_1},\ f_9=\frac{\beta T_0\chi_1 d}{\rho c_1^2 b_1},\ f_{10}=\frac{a_3c_1^2}{\omega_1^2 b_1},\ f_{11}=\frac{a_2c_1^2}{\omega_1^2 b_1},\ f_{12}=\frac{\gamma_2T_0\chi_1}{b_1},$$

$$f_{13}=\frac{\gamma_1c_1^4}{K\omega_1^3\chi_1},\ f_{14}=\frac{\gamma_2c_1^4}{K\omega_1^3\chi_1},\ \varepsilon=\frac{\beta^2T_0}{\rho C_e(\lambda+2\mu)},\ c_1^2=\frac{\lambda+2\mu}{\rho},\ \omega_1=\frac{C_e\rho c_1^2}{K},$$

$$c_3^2=\frac{a}{\chi_1},\ c_2^2=\frac{\mu}{\rho},\ c_4^2=\frac{b_1}{\chi_2},\delta^2=\frac{c_2^2}{c_1^2},\ \delta_1^2=\frac{c_3^2}{c_1^2},\ \delta_2^2=\frac{c_4^2}{c_1^2}.$$

Here, ε denotes the constant for thermomechanical coupling, ω_1 denotes the characteristics frequency, $c_i;\, i=1,2,3,4$ are the velocities due to longitudinal wave, transverse wave, and volume fraction fields of dual voids, respectively.

Now, using the Helmholtz theorem, we have

$$w=G,_z-H,_x\,,\ u=G,_x+H,_z \tag{3.12}$$

here, *G* and *H* represent the scalar and vector velocity potential functions. Equations (3.7)–(3.11), combined with equation (3.12), yield the following results.

$$G,_{xx}+G,_{zz}+f_1\phi+f_2\psi-T=(1-\xi^2\nabla^2)\ddot{G} \tag{3.13}$$

$$\delta^2(H,_{xx}+H,_{zz})=(1-\xi^2\nabla^2)\ddot{H} \tag{3.14}$$

$$-f_4(G,_{xx}+G,_{zz})+f_3(\psi,_{xx}+\psi,_{zz})-f_5\phi+\phi,_{xx}+\phi,_{zz}-f_6\psi+f_7T=\frac{1}{\delta_1^2}(1-\xi^2\nabla^2)\ddot{\phi} \tag{3.15}$$

$$-f_9(G,_{xx}+G,_{zz})+f_8(\psi,_{xx}+\psi,_{zz})-f_{10}\phi+\phi,_{xx}+\phi,_{zz}-f_{11}\psi+f_{12}T=\frac{1}{\delta_2^2}(1-\xi^2\nabla^2)\ddot{\psi} \tag{3.16}$$

$$(1+\tau_TD_{\tau_T})(T,_{xx}+T,_{zz})=\left(1-\xi^2\nabla^2+\tau_qD_{\tau_q}+a_0\frac{\tau_q^2}{2}D_{\tau_q}^2\right)(\varepsilon(\dot{G},_{xx}+\dot{G},_{zz})+f_{13}\dot{\phi}+f_{14}\dot{\psi}+\dot{T}) \tag{3.17}$$

Following Achenbach [21], for the inviscid fluid half-space, the governing equations are

$$p_f = -\rho_f \dot{\phi}_f \tag{3.18}$$

$$\left(\nabla^2 - \frac{1}{\alpha_f^2} \frac{\partial}{\partial t^2} \right) \phi_f = 0 \tag{3.19}$$

$$\vec{u}_f = \nabla \phi_f \tag{3.20}$$

Where, $\alpha_f^2 = \frac{\lambda_f}{\rho_f}$, p_f represents the acoustic pressure, ρ_f is density, λ_f is the bulk modulus, u_f, w_f are velocity components, ϕ_f is the velocity potential of the fluid medium.

Upon incorporating the dimensionless quantities as per equation (3.6) and omitting the primes, we get

$$\left(\nabla^2 - \frac{1}{\delta_f^2} \frac{\partial}{\partial t^2} \right) \phi_f = 0, \text{ where, } \delta_f^2 = \frac{\alpha_f^2}{c_1^2}. \tag{3.21}$$

4. The problem's solution

Utilizing the eigenmode technique, we assume the following solutions:

$$(\psi, T, \phi_f, G, H, \phi) = \{\bar{\psi}(z), \bar{T}(z), \bar{\phi}_f(z), \bar{G}(z), \bar{H}(z), \bar{\phi}(z)\} \exp\{\iota k(x - ct)\} \tag{4.1}$$

Where bar notations denote the amplitudes of the respective functions, ω and k are the angular velocity and the wavenumber, and $c = \omega / k$ is the phase velocity.

After using equation (4.1), equations (3.13)-(3.17) and (3.21) take the form (after suppressing the bars):

$$(d_{11} + d_{12} m^2) G + f_1 \phi + f_2 \psi - T = 0 \tag{4.2}$$

$$(-f_4 m^2 + d_{31}) G + (d_{32} m^2 + d_{33}) \phi + (f_3 m^2 - d_{34}) \psi + f_7 T = 0 \tag{4.3}$$

$$(-f_9 m^2 + d_{41}) G + (m^2 - d_{42}) \phi + (d_{43} m^2 + d_{44}) \psi + f_{12} T = 0 \tag{4.4}$$

$$(d_{52} m^4 + d_{53} m^2 + d_{54}) G + (d_{55} m^2 + d_{56}) \phi + (d_{57} m^2 + d_{58}) \psi + (d_{59} m^2 + d_{60}) T = 0 \tag{4.5}$$

$$(m^2 - m_5^2)H = 0 \tag{4.6}$$

$$(m^2 - m_6^2)\phi_f = 0 \tag{4.7}$$

Where, $m = \dfrac{d}{dz}$, $d_{11} = k^2(c^2 - 1 + \omega^2\xi^2)$, $d_{12} = 1 - \xi^2 c^2 k^2$, $d_{31} = f_4 k^2$,

$d_{32} = 1 - \dfrac{\omega^2\xi^2}{\delta_1^2}$ $d_{33} = k^2\left(\dfrac{c^2}{\delta_1^2} - 1 + \dfrac{\xi^2\omega^2}{\delta_1^2}\right) - f_5$, $d_{34} = f_3 k^2 + f_6$, $d_{41} = f_9 k^2$,

$d_{42} = k^2 + f_{10}$, $d_{43} = f_8 - \dfrac{\omega^2\xi^2}{\delta_2^2}$, $d_{44} = k^2\left(\dfrac{c^2}{\delta_2^2}(1 - \xi^2 k^2) - f_8\right) - f_{11}$,

$A_1 = \left(1 + \tau_q \mathrm{E}(\tau_q, Q) + a_0 \dfrac{\tau_q^2}{2}\mathrm{E}^2(\tau_q, Q)\right)$, $A_2 = 1 + \tau_T \mathrm{E}(\tau_T, Q)$, $A_3 = A_1 / A_2$,

$A_4 = \xi^2 / A_2$, $d_{52} = -\iota kc\varepsilon A_4$, $d_{53} = \iota kc\varepsilon(d_{51} + k^2 A_4)$, $d_{54} = -k^3 \iota c\varepsilon d_{51}$,

$d_{55} = -f_{13}\iota kcA_4$, $d_{56} = \iota kcf_{13}d_{51}$, $d_{57} = -\iota kcf_{14}A_4$, $d_{58} = f_{14}\iota kcd_{51}$, $d_{59} = 1 - \iota kcA_4$,

$d_{60} = \iota kcd_{51} - k^2, Q = \iota\omega$

$$\mathrm{E}(\tau_i, Q) = \frac{\{-(m^2 - 2n + 1)Q^2\tau_i^2 + 2Q\tau_i^2(m^2 - n) + 2m^2\}\exp(-Q\tau_i) + Q^2\tau_i^2 - 2Qn\tau_i + 2m^2}{\tau_i^3 Q^2}; i = q, T.$$

For the nontrivial solutions, equations (4.2)-(4.5) yield the following characteristics equation

$$L_0 m^8 + L_1 m^6 + L_2 m^4 + L_3 m^2 + L_4 = 0 \tag{4.8}$$

The coefficients $L_i : i = 0 - 4$ are determined using the determinant of equations (4.2)-(4.5), roots $m_j^2\,(j = 1 - 4)$ are determined by solving equation (4.8).

Characteristics roots of the equation (4.6) are

$$m_5^2 = k^2\left(1 - \frac{c^2}{\delta^2 - \omega^2\xi^2}\right) \tag{4.9}$$

The mechanical wave in the fluid medium is represented by equation (3.21), having the characteristic root.

$$m_6^2 = k^2\left(1-\frac{c^2}{\delta_f^2}\right) \tag{4.10}$$

The radiation condition $\mathrm{Re}(m_j \geq 0, j=1-5)$, for the medium M_1, is satisfied by the solution

$$(G,\phi,\psi,T) = \sum_{j=1}^{4}(1,V_j,W_j,S_j)U_j \exp\{\iota k(x-ct)-m_j z\} \tag{4.11}$$

$$H = U_5 \exp\{\iota k(x-ct)-m_5 z\} \tag{4.12}$$

For the medium M_2, the radiation conditions $\mathrm{Re}(m_6) \geq 0$ is satisfied by the solution is given

$$\phi_f = U_6 \exp\{\iota k(x-ct)+m_6 z\} \tag{4.13}$$

By substituting the value of the solution (4.11) into the equations (3.13), (3.15), and (3.16), a nonlinear set of equations is obtained. The collection of equations can be shown as a matrix as follows:

$$\begin{bmatrix} f_1 & f_2 & -1 \\ m_q^2 d_{32}+d_{33} & f_3 m_q^2 - d_{34} & f_7 \\ m_q^2 - d_{42} & m_q^2 d_{43}+d_{44} & f_{12} \end{bmatrix}\begin{bmatrix} V_j \\ W_j \\ S_j \end{bmatrix} = \begin{bmatrix} -m_q^2 d_{12} - d_{11} \\ f_4 m_q^2 - d_{31} \\ f_9 m_q^2 - d_{41} \end{bmatrix} \tag{4.14}$$

The values of parameters V_j, W_j, S_j are obtained from equation (4.14).

5. Conditions at the Boundary

The boundary conditions are assumed at $z=0$ as follows;

$$\sigma_{zz}^L = -p_f,\ \sigma_{zx}^L = 0,\ \sigma_{zz}^L = K_n\left(w_f - \frac{\partial w}{\partial t}\right),\ (\zeta_z^1)^L = 0,\ (\zeta_z^2)^L = 0,\ T,_z + H^* T = 0 \tag{5.1}$$

it is noted that H^* indicated heat coefficient and K_n indicated stiffness parameter. The given boundary conditions may be written with potential functions using the constitutive relations as follows

$$(1-\xi^2\nabla^2)\ddot{G} - 2\delta^2(G,_{xx} + H,_{xz}) = \frac{\rho_f c_1^2}{\beta T_0}\dot{\phi}_f \tag{5.2}$$

$$(1-\xi^2\nabla^2)\ddot{H}+2\delta^2(G,_{xz}-H,_{xx})=0 \tag{5.3}$$

$$(1-\xi^2\nabla^2)\ddot{G}-2\delta^2(G,_{xx}+H,_{xz})=\frac{K_n c_1}{\beta T_0}\phi_{f,z}-\frac{K_n c_1}{\lambda+2\mu}(\dot{G},_z-\dot{H},_x) \tag{5.4}$$

$$a\phi,_z+b_1\psi,_z=0 \tag{5.5}$$

$$b_1\phi,_z+\gamma\psi,_z=0 \tag{5.6}$$

$$T,_z+H^*T=0 \tag{5.7}$$

6. Derivation of the secular equation

After putting the solutions (4.11)-(4.13) in the equations (5.2)-(5.7), we get a set of equations in $U_q, q=(1-6)$ as

$$\sum_{q=1}^{4}(p_{11}+p_{12}m_q^2)U_q+p_{13}m_5U_5+p_{14}U_6=0 \tag{6.1}$$

$$\sum_{q=1}^{4}-p_{13}m_qU_q+(p_{11}+p_{12}m_5^2)U_5=0 \tag{6.2}$$

$$\sum_{q=1}^{4}(p_{11}+p_{31}m_q+p_{32}m_q^2)U_q+(p_{33}+p_{34}m_5)U_5+p_{35}m_6U_6=0 \tag{6.3}$$

$$\sum_{q=1}^{4}m_q(V_q+f_3W_q)U_q=0 \tag{6.4}$$

$$\sum_{q=1}^{4}m_q(V_q+f_8W_q)U_q=0 \tag{6.5}$$

$$\sum_{q=1}^{4}(m_q+H^*)S_qU_q=0 \tag{6.6}$$

where, $p_{11}=-\omega^2(1+k^2\xi^2)+2k^2\delta^2$, $p_{12}=\omega^2\xi^2$, $p_{13}=2\delta^2\iota k$, $p_{14}=\iota kc\dfrac{\rho_f c_1^2}{\beta T_0}$,

$$p_{31}=\frac{\iota kcK_n}{\rho c_1},\ p_{32}=\omega^2\xi^2,\ p_{33}=\frac{-K_nk^2c}{\rho c_1},\ p_{34}=2\delta^2\iota k,\ p_{35}=\frac{-K_nc_1}{\beta T_0}.$$

Using the set of equations (6.1)-(6.6) and upon doing algebraic calculations, the ensuing secular equation is obtained as

$$\begin{aligned}
&p_{14}(p_{11}+p_{12}m_5^2)[(p_{11}+p_{31}m_1+p_{32}m_1^2)(F_1+H^*F_1')-(p_{11}+p_{31}m_2+p_{32}m_2^2)\\
&(F_2+H^*F_2')+(p_{11}+p_{31}m_3+p_{32}m_3^2)(F_3+H^*F_3')-(p_{11}+p_{31}m_4+p_{32}m_4^2)\\
&(F_4+H^*F_4')]+(p_{14}p_{13}(p_{33}+p_{34}m_5)-p_{35}p_{13}^2.m_5m_6)[m_1(F_1+H^*F_1')-\\
&m_2(F_2+H^*F_2')+m_3(F_3+H^*F_3')-m_4(F_4+H^*F_4')]-p_{35}m_6(p_{11}+p_{12}m_5^2)\\
&[(p_{11}+p_{12}m_1^2)(F_1+H^*F_1')-(p_{11}+p_{12}m_2^2)(F_2+H^*F_2')+(p_{11}+p_{12}m_3^2)(F_3+H^*F_3')\\
&-(p_{11}+p_{12}m_4^2)(F_4+H^*F_4')]=0
\end{aligned}\tag{6.7}$$

where,

$$F_1=\begin{vmatrix} m_2(V_2+f_3W_2) & m_3(V_3+f_3W_3) & m_4(V_4+f_3W_4)\\ m_2(V_2+f_8W_2) & m_3(V_3+f_8W_3) & m_4(V_4+f_8W_4)\\ m_2S_2 & m_3S_3 & m_4S_4\end{vmatrix},$$

$$F_2=\begin{vmatrix} m_1(V_1+f_3W_1) & m_3(V_3+f_3W_3) & m_4(V_4+f_3W_4)\\ m_1(V_1+f_8W_1) & m_3(V_3+f_8W_3) & m_4(V_4+f_8W_4)\\ m_1S_1 & m_3S_3 & m_4S_4\end{vmatrix},$$

$$F_3=\begin{vmatrix} m_1(V_1+f_3W_1) & m_2(V_2+f_3W_2) & m_4(V_4+f_3W_4)\\ m_1(V_1+f_8W_1) & m_2(V_2+f_8W_2) & m_4(V_4+f_8W_4)\\ m_1S_1 & m_2S_2 & m_4S_4\end{vmatrix},$$

$$F_4=\begin{vmatrix} m_1(V_1+f_3W_1) & m_2(V_2+f_3W_2) & m_3(V_3+f_3W_3)\\ m_1(V_1+f_8W_1) & m_2(V_2+f_8W_2) & m_3(V_3+f_8W_3)\\ m_1S_1 & m_2S_2 & m_3S_3\end{vmatrix}.$$

Similarly, F_q' can be derived by substituting m_qS_q to S_q in F_q, $q=1-4$.

7. Solving the secular equation

The characteristic equation (6.7) provide all of the information regarding the wave attributes, including wavenumber, attenuation coefficient, and phase velocity. The characteristic equation (4.8) has roots in complex quantities. Thus, the waves' phase velocity is similarly complex. After obtaining the characteristic roots $m_j^2; j = 1-6,$ we get

$$c_j = \pm\frac{1}{m_j}. \tag{7.1}$$

We write $c_j^{-1} = v_j^{-1} + \iota\omega^{-1}Q_j^*$ (7.2)

noted that $k = R_j^* + \iota\omega^{-1}Q_j^*$, $R_j^* = \omega/v_j$, and Q_j^* are real quantities. Equation (4.1) provides the component of the solution that becomes $-Q_j^*x + \iota R_j^*(x - v_j t)$. This implies that Q_j^* and v_j are the wave attenuation coefficient and phase velocity. Using equations (6.7) and (7.2), the MATLAB software is used to obtain the roots $m_j^2\,(j = 1-4)$ of the characteristic equation (4.8). By using m_j^2, once the characteristic equation (6.7) is solved, and putting relation (7.2) in equation (7.1), phase velocity (v_j) and attenuation coefficient (Q_j^*) of waves is determined as $v_j = 1/\mathrm{Re}(m_j)$, $Q_j^* = \omega\,\mathrm{Im}(m_j)$; $j = 1-4$. Specific loss is described as the ratio of the energy dissipated (ΔE) in a material during one complete stress cycle to the maximum energy stored in the specimen at its peak strain (E). Here, the specific loss is

$$SL = \left|\frac{\Delta E}{E}\right| = 4\pi\left|\frac{\mathrm{Im}(k)}{\mathrm{Re}(k)}\right| = 4\pi\left|\frac{Q_j^*}{R_j^*}\right| = 4\pi\left|\frac{v_j\,Q_j^*}{\omega}\right| \tag{7.3}$$

The penetrating depth of the waves is given as

$$PD = \frac{1}{|\mathrm{Im}(k)|} = \frac{1}{|Q_j^*|}. \tag{7.4}$$

8. Physical field's distribution

Using the interface's boundary conditions (5.1) of the nonlocal isotropic thermoelastic solid and inviscid fluid half-spaces, the components of displacement, fluid displacement, variation in temperature, and fraction of volume field have been determined. From the equations (5.2)-(5.7), we have

$$\tilde{U}_s = U_s\Omega\,\exp(\wp_j),\ \tilde{W}_s = W_s\Omega\,\exp(\wp_j),\ \tilde{\phi}_s = \Phi\,\Omega\,\exp(\wp_j),\ \tilde{\psi}_s = \Psi\,\Omega\,\exp(\wp_j),$$

$$\tilde{T}_s = \Theta\,\Omega\,\exp(\wp_j),\ \tilde{U}_f = U_f\Omega\,\exp(\wp_j),\ \tilde{W}_f = W_f\,\Omega\,\exp(\wp_j),$$

$$(\wp_j) = \iota R_j^*(x - v_j^* t); j = 1 - 6 \tag{8.1}$$

Here, $u = \tilde{U}_s, w = \tilde{W}_s, \phi = \tilde{\phi}_s, \psi = \tilde{\psi}_s, T = \tilde{T}_s, u_f = \tilde{U}_f, w_f = \tilde{W}_f$ at $z = 0$ and

$\Omega = U_1 \exp\{-Q_j^* x\}$, $U_S = \iota k\left(1 + \sum_{i=2}^{4} \frac{U_i}{U_1}\right) - m_5 \frac{U_5}{U_1}$, $W_S = -\left(m_1 + + \sum_{i=2}^{4} \frac{m_i U_i}{U_1} + \iota k \frac{U_5}{U_1}\right)$,

$\Phi = V_1 + + \sum_{i=2}^{4} \frac{V_i U_i}{U_1}$, $\Psi = W_1 + \sum_{i=2}^{4} \frac{W_i U_i}{U_1}$, $\Theta = S_1 + \sum_{i=2}^{4} \frac{S_i U_i}{U_1}$, $U_f = \iota k \frac{U_6}{U_1}$, $W_f = m_6 \frac{U_6}{U_1}$.

Inserting equation (8.1) in the set of equations (5.2)-(5.7), we get

$$AX = B \tag{8.2}$$

where,

$$A = \begin{bmatrix} p_{11} + p_{12}m_2^2 & p_{11} + p_{12}m_3^2 & p_{11} + p_{12}m_4^2 & p_{13}m_5 & p_{14} \\ -p_{13}m_2 & -p_{13}m_3 & -p_{13}m_4 & p_{11} + p_{12}m_5^2 & 0 \\ p_{11} + p_{31}m_2 + p_{32}m_2^2 & p_{11} + p_{31}m_3 + p_{32}m_3^2 & p_{11} + p_{31}m_4 + p_{32}m_4^2 & p_{33} + p_{34}m_5 & p_{35}m_6 \\ m_2(V_2 + f_3W_2) & m_3(V_3 + f_3W_3) & m_4(V_4 + f_3W_4) & 0 & 0 \\ m_2(V_2 + f_8W_2) & m_3(V_3 + f_8W_3) & m_4(V_4 + f_8W_4) & 0 & 0 \end{bmatrix}$$

$$X = \begin{bmatrix} U_2/U_1 \\ U_3/U_1 \\ U_4/U_1 \\ U_5/U_1 \\ U_6/U_1 \end{bmatrix}, B = \begin{bmatrix} -p_{11} - p_{12}m_1^2 \\ p_{13}m_1 \\ -\left(p_{11} + p_{31}m_1 + p_{32}m_1^2\right) \\ -m_1\left(V_1 + f_3W_1\right) \\ -m_1\left(V_1 + f_8W_1\right) \end{bmatrix}$$

Equation 8.2 is used to determine the value of $U_i / U_1 (i = 2 - 6)$.

9. Numerical Results and Discussions

Utilizing the MATLAB software, a numerical analysis is conducted to illustrate how the memory-dependent derivative, nonlocal parameter, and stiffness parameter impact a range of wave profiles. The computation takes into account a substance that resembles magnesium crystals. Following Pathania and Joshi [22] and Singh and Tomar [23], numerical values are given in Table 1.

Table 1

Material constant values

Symbol	Value	Symbol	Value
λ	$1.5\times10^{10}\,Nm^{-2}$	γ_2	$3.11\times10^{6}\,Nm^{-2}$
a_1	$1.2\times10^{10}\,Nm^{-2}$	C_e	$1.809\times10^{6}\,m^2s^2K^{-1}$
μ	$7.5\times10^{9}\,Nm^{-2}$	K	$1.7\times10^{2}\,Wm^{-1}K^{-1}$
a_3	$1.23\times10^{6}\,Nm^{-2}$	ρ_f	$1.0\times10^{3}\,Kgm^{-3}$
b	$2\times10^{8}\,Nm^{-2}$	d	$2.1\times10^{8}\,Nm^{-2}$
ρ	$2\times10^{3}\,Kgm^{-3}$	b_1	$8.1\times10^{6}\,N$
a_2	$2.21\times10^{10}\,Nm^{-2}$	a	$8\times10^{9}\;N$
T_0	$293\;K$	χ_2	$330\,kgm^{-1}$
α_t	$1.78\times10^{-5}\,K^{-1}$	λ_f	$2.140\times10^{3}\,Nm^{-2}$
γ	$8.2\times10^{9}\,N$	χ_1	$320\,kgm^{-1}$
γ_1	$2\times10^{6}\,Nm^{-2}K^{-1}$		

For numerical computations, values of nonlocal and phase lags are considered as $\xi = 0.002$, $\tau_T = 0.1s$, and $\tau_q = 0.4s$ for a fixed kernel $k(t-\xi) = 1-(t-\xi)/\tau$. Figs. 2-12 represent the impact of memory and nonlocality on the considered model. The thermoelastic solid with MDD, nonlocal thermoelastic solid with MDD, and nonlocal thermoelastic solid without MDD models are shown by the blue, red, and green solid lines, respectively.

The relationship between the wavenumber and the phase velocity profile is shown in Fig. 2. The phase velocity decreases with increasing wavenumber. All three curves initially line up, but when the wavenumber rises, there is a noticeable variance for all models considered. It has been observed that the amplitude of phase velocity increases when nonlocality is present.

Fig. 3 shows how wavenumber affects specific loss. When the wavenumber is less, the magnitude of specific loss is higher and decreases as it increases. When the wavenumber rises, there is a noticeable variation for every model considered, even if the three curves initially coincide. It has been demonstrated that the amplitude of phase velocity grows when MDD is present and decreases when nonlocality is present.

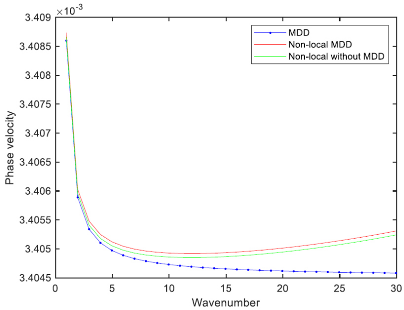

Figure 2

Variation of phase velocity with wavenumber

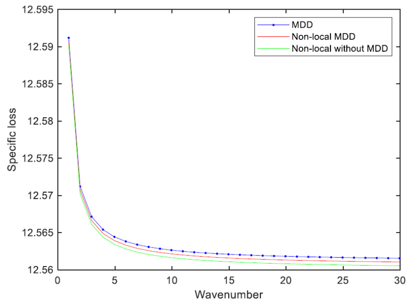

Figure 3

Variation of specific loss with wavenumber

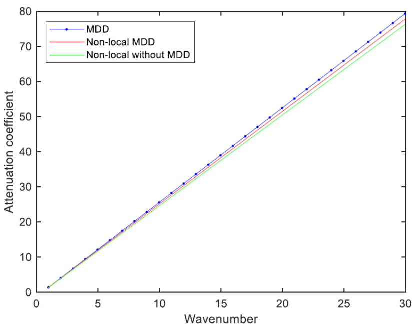

Figure 4

Variation of attenuation coefficient with wavenumber

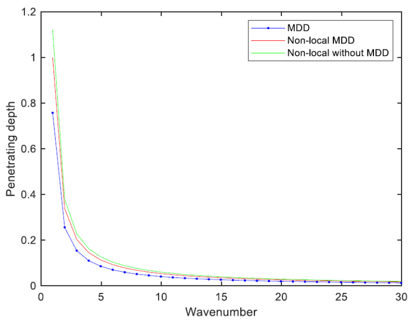

Figure 5

Variation of penetrating depth with wavenumber

The attenuation coefficient's behavior with wavenumber is depicted in Fig. 4. The attenuation coefficient clearly rises linearly with wave number, as the graph shows. The effect of MDD and nonlocality on the attenuation coefficient is nearly identical to that seen in the specific loss graph in Fig. 3. The relationship between the penetration depth and wavenumber is demonstrated in Fig. 5. For vanishing wavenumber, the penetrating depth magnitude is rather great, and it decreases with increasing wavenumber. At first, the presence of MDD causes a fall in penetrating depth, and the presence of nonlocality causes an increase in magnitude. As a further increase of wavenumber, all three curves overlap and disappear the impact of MDD and nonlocality.

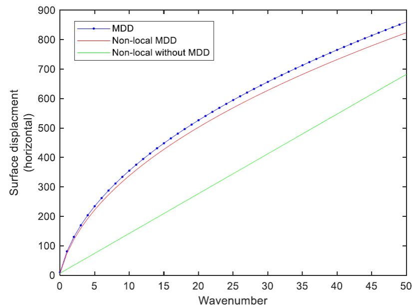

Figure 6

Variation of surface displacement (horizontal) with wavenumber

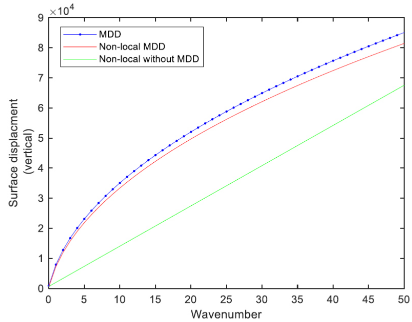

Figure 7

Variation of surface displacement (vertical) with wavenumber

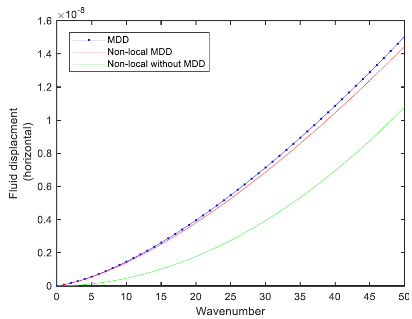

Figure 8

Variation of fluid displacement (horizontal) with wavenumber

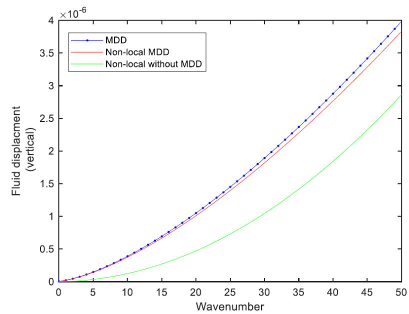

Figure 9

Variation of fluid displacement (vertical) with wavenumber

The visual representations of the components of horizontal and vertical surface displacement with wavenumber are presented in Figs. 6 and 7, respectively. The surface displacement components are reduced when MDD is absent and nonlocality is present. Surface displacement components have a nearly linear pattern in the absence of MDD with nonlocality. Figs. 8 and 9 demonstrate how the wavenumber affects both the horizontal displacement components and the components of vertical fluid displacement. Although the fluid displacement components are shown to roughly follow the same pattern for the models under consideration, their magnitudes vary.

The impact of the wavenumber on temperature change at the solid-fluid half-space interface is presented in Fig. 10. As the wavenumber rises, so does the change in surface temperature. With MDD present, the surface temperature variation shows a greater magnitude and follows a linear trend. Nonlocality makes the shift in surface temperature less drastic.

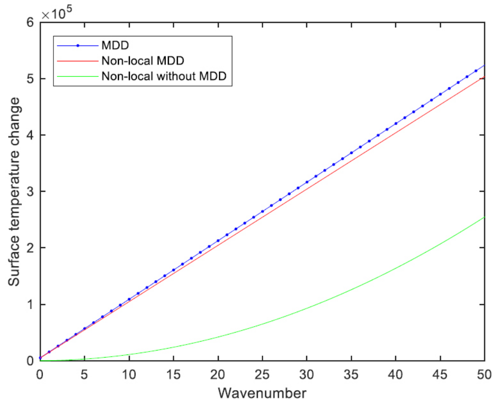

Figure 10

Variation of surface temperature change with wavenumber

Figs. 11 and 12 depict the changes in the volume fraction field for type-I and type-II voids concerning the wavenumber. An exponential decrease in the volume fraction of both void types is observed as the wavenumber increases. The volume fraction field influenced by voids becomes more significant in the presence of MDD and nonlocal effects.

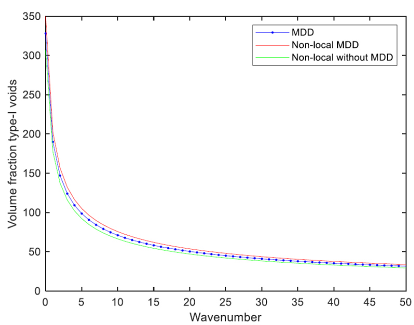

Figure 11

Variation of Volume fraction type I voids with wavenumber

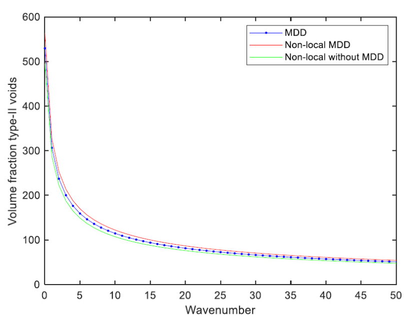

Figure 12

Variation of Volume fraction type II voids with wavenumber

Figs. 13-23 represent the impact of stiffness parameters on the considered model. The stiffness parameter $K_n = 5$, $K_n = 10$, and $K_n \to \infty$ are shown by the blue, red, and green solid lines, respectively.

The impact of the stiffness parameter on the variation of wave phase velocity is shown in Fig. 13. It has been found that as the stiffness parameter value rises, phase velocity increases in magnitude as well. If the stiffness parameter value tends to infinity, i.e., the interface is perfect, the amplitude of phase velocity is higher than when the interface is imperfect, i.e., the waves travel more efficiently at a perfect interface than at the imperfect interface.

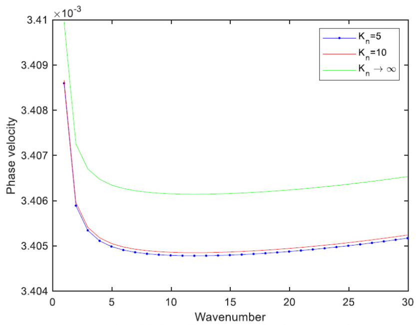

Figure 13

Variation of phase velocity with wavenumber

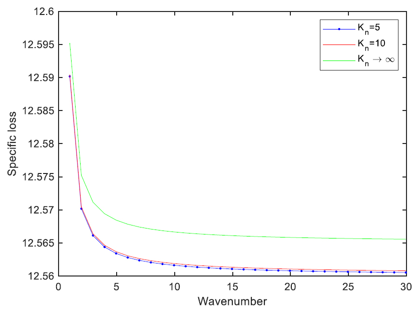

Figure 14

Variation of specific loss with wave-number

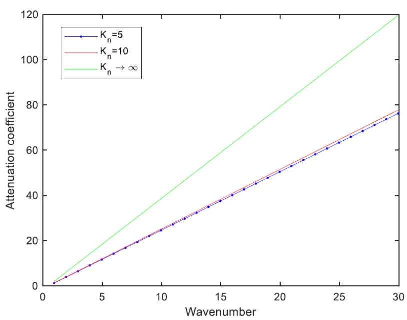

Figure 15

Variation of attenuation coefficient with wavenumber

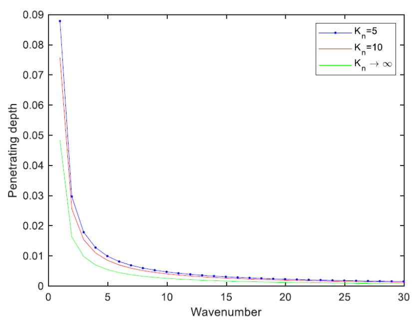

Figure 16

Variation of penetrating depth with wavenumber

Fig.14 shows the impact of the stiffness parameter on the specific loss. As the wavenumber increases, the specific loss magnitude diminishes. Furthermore, when the stiffness parameter value diminishes, the amplitude of a specific loss also decreases. A perfect interface results in a greater magnitude of specific loss than an imperfect interface.

Fig. 15 shows the relationship between the attenuation coefficient and wavenumber for various stiffness parameter values. The attenuation coefficient's amplitude consistently grows with increasing wavenumber, and it similarly rises with higher stiffness parameter values. Notably, there is a substantial difference in the magnitude of the attenuation coefficient between perfect and imperfect interfaces. In imperfect interfaces, the magnitude is lower compared to perfect interfaces.

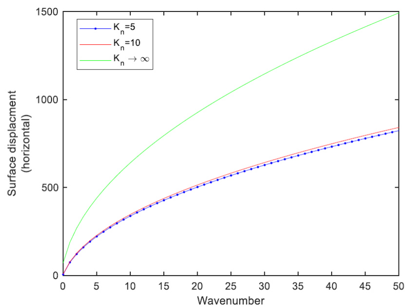

Figure 17

Variation of surface displacement (horizontal) with wavenumber

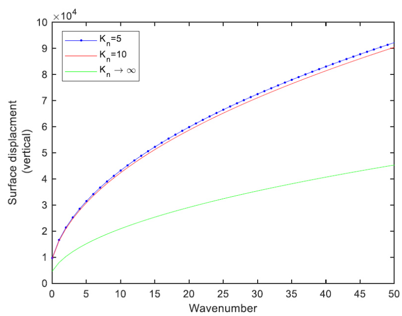

Figure 18

Variation of surface displacement (vertical) with wavenumber

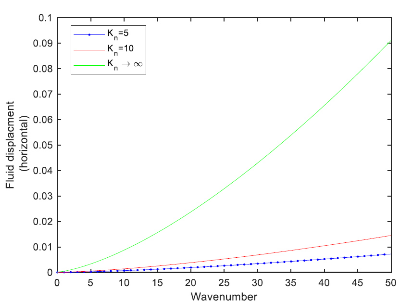

Figure 19

Variation of fluid displacement (horizontal) with wavenumber

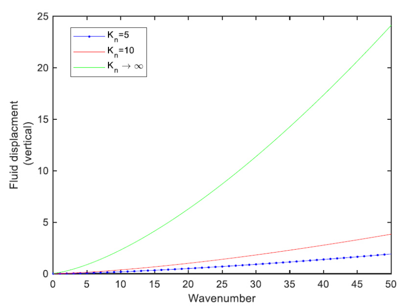

Figure 20

Variation of fluid displacement (vertical) with wavenumber

Fig. 16 illustrates the effect of stiffness parameters on the depth corresponding to the wavenumber. A larger value of the stiffness parameter corresponds to a lower magnitude of the penetration depth. Also, if the stiffness parameter's value is approaching infinite, i.e., the interface is perfect, the penetrating depth's magnitude is lower compared to the imperfect interface.

Figs. 17 and 18 show how the stiffness parameters affect the surface displacements in the horizontal and vertical directions. The magnitude of the horizontal displacement component increases as the stiffness parameter's value increases while the amplitude of the vertical displacement component decreases. The amplitude of the horizontal surface displacement component is higher when the interface is perfect compared to when it is imperfect, while the magnitude of the vertical displacement component exhibits the opposite pattern.

The influence of the stiffness parameter on the vertical and horizontal fluid displacement components' magnitude is shown in Figs. 19 and 20, respectively. For all the values of the stiffness parameter considered, both the fluid displacement components rise with the wavenumber. The magnitude of the fluid's components of displacement increases along with the stiffness parameter's value. The magnitude of both displacement components is more prominent when it comes to a perfect interface than it is in the case of an imperfect interface.

Fig. 21 depicts the change in surface temperature with wave number for various stiffness parameter values. The stiffness parameter acts as an

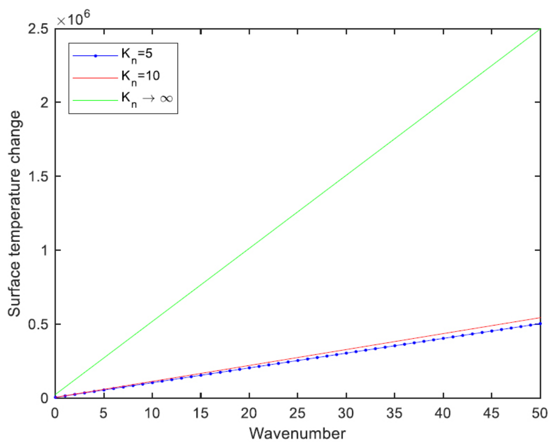

Figure 21

Variation of surface temperature change with wavenumber

increasing agent for the surface temperature change's amplitude. When the interface is perfect, i.e., when the stiffness parameter value tends to infinity, the surface temperature amplitude is much higher than when the interface is imperfect.

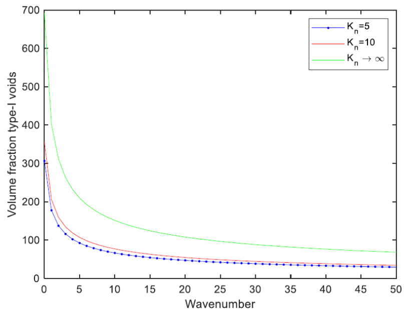

Figure 22

Variation of Volume fraction type I voids with wavenumber

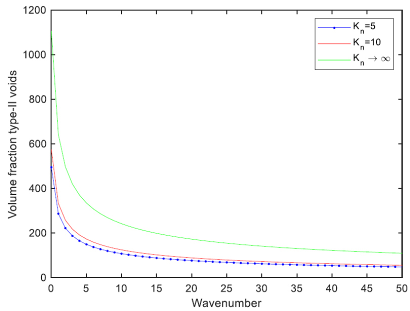

Figure 23

Variation of Volume fraction type II voids with wavenumber

Figs. 22 and 23 show the influence of stiffness parameters on the variation in fraction of volume for type-I and type-II voids. The fraction of volume associated with both types of voids decreases due to the wavenumber increases. Additionally, an increase in the stiffness parameter value results in higher volume fraction fields for both types of voids. If the stiffness parameter tends to infinity, the volume fraction field's magnitude also increases.

10. Conclusion

In the current study, plane wave propagation at the surface of an isotropic homogeneous nonlocal thermoelastic solid-half space having double porosity with memory-dependent derivative (MDD) and inviscid fluid half-space. From the above analytical and numerical discussion, some significant observations concluded as

- When nonlocal effects are present, the magnitudes of the attenuation coefficient, solid displacement, fluid displacement, and temperature change decrease, whereas the phase velocity and penetrating depth increase.
- The amplitude of specific loss, attenuation coefficient, phase velocity, change in temperature, and components of displacement is higher

when memory effect is present, while the magnitude of penetrating depth shows a lower amplitude.

- In contrast to the nonlocal effect, the memory-dependent derivative effect enhances the magnitude fraction of volume field for both kinds of voids.
- The amplitude of the attenuation coefficient, phase velocity, specific loss, temperature change, horizontal and vertical fluid displacements, and void's volume fraction field increases as the value of the stiffness parameter increases, but the amplitude of penetrating depth decreases.
- The amplitude of the horizontal solid displacement component increases as the stiffness parameter's value rises, while the magnitude of the vertical solid displacement component decreases.

Disclosure statement

The authors have no conflict of interest.

References

[1] D. G. B. Edelen and N. Laws, 'On the thermodynamics of systems with nonlocality', *Arch. Ration. Mech. Anal.*, vol. 43, no. 1, pp. 24–35 (1971), doi: 10.1007/BF00251543.

[2] A. C. Eringen and D. G. B. Edelen, 'On nonlocal elasticity', *Int. J. Eng. Sci.*, vol. 10, no. 3, pp. 233–248, Mar. (1972), doi: 10.1016/0020-7225(72)90039-0.

[3] C. Polizzotto, 'Nonlocal elasticity and related variational principles', *Int. J. Solids Struct.*, vol. 38, no. 42–43, pp. 7359–7380 (2001), doi: 10.1016/S0020-7683(01)00039-7.

[4] A. Chakraborty, 'Wave propagation in anisotropic media with non-local elasticity', *Int. J. Solids Struct.*, vol. 44, no. 17, pp. 5723–5741 (2007), doi: 10.1016/j.ijsolstr.2007.01.024.

[5] R. Kumar, A. K. Vashishth, and S. Ghangas, 'Nonlocal heat conduction approach in a bi-layer tissue during magnetic fluid hyperthermia with dual phase lag model', *Biomed. Mater. Eng.*, vol. 30, no. 4, pp. 387–402 (2019), doi: 10.3233/BME-191061.

[6] J.-L. Wang and H.-F. Li, 'Surpassing the fractional derivative: Concept of the memory-dependent derivative', *Comput. Math. with*

Appl., vol. 62, no. 3, pp. 1562–1567, Aug. (2011), doi: 10.1016/j.camwa.2011.04.028.

[7] M. Caputo and F. Mainardi, 'A new dissipation model based on memory mechanism', *Pure Appl. Geophys.*, vol. 91, no. 1, pp. 134–147 (1971).

[8] J. W. Nunziato and S. C. Cowin, 'A nonlinear theory of elastic materials with voids', *Arch. Ration. Mech. Anal.*, vol. 72, no. 2, pp. 175–201 (1979), doi: 10.1007/BF00249363.

[9] D. Ieşan, 'A theory of thermoelastic materials with voids', *Acta Mech.*, vol. 60, no. 1, pp. 67–89 (1986).

[10] D. Ieşan and R. Quintanilla, 'On a theory of thermoelastic materials with a double porosity structure', *J. Therm. Stress.*, vol. 37, no. 9, pp. 1017–1036 (2014), doi: 10.1080/01495739.2014.914776.

[11] V. Gupta, R. Kumar, M. Kumar, V. Pathania, and M. S. Barak, 'Reflection/transmission of plane waves at the interface of an ideal fluid and nonlocal piezothermoelastic medium', *Int. J. Numer. Methods Heat Fluid Flow*, vol. 33, no. 2, pp. 912–937, Jan. (2023), doi: 10.1108/HFF-04-2022-0259.

[12] M. S. Barak, R. Kumar, R. Kumar, and V. Gupta, 'The effect of memory and stiffness on energy ratios at the interface of distinct media', *Multidiscip. Model. Mater. Struct.*, vol. 19, no. 3, pp. 464–492 (2023), doi: 10.1108/MMMS-10-2022-0209.

[13] V. Gupta, R. Kumar, R. Kumar, and M. S. Barak, 'Energy analysis at the interface of piezo/thermoelastic half spaces', *Int. J. Numer. Methods Heat Fluid Flow*, vol. 33, no. 6, pp. 2250–2277, May (2023), doi: 10.1108/HFF-11-2022-0654.

[14] M. S. Barak, R. Kumar, R. Kumar, and V. Gupta, 'The effect of memory and stiffness on energy ratios at the interface of distinct media', *Multidiscip. Model. Mater. Struct.*, vol. 19, no. 3, pp. 464–492, Apr. (2023), doi: 10.1108/MMMS-10-2022-0209.

[15] V. Gupta and M. S. Barak, 'Quasi-P wave through orthotropic piezo-thermoelastic materials subject to higher order fractional and memory-dependent derivatives', *Mech. Adv. Mater. Struct.*, vol. 0, no. 0, pp. 1–15, Jun. (2023), doi: 10.1080/15376494.2023.2217420.

[16] V. Pathania, R. Kumar, V. Gupta, and M. S. Barak, 'Generalized Plane Waves in a Rotating Thermoelastic Double Porous Solid', *Int. J. Appl.*

Mech. Eng., vol. 27, no. 4, pp. 138–154, Dec. (2022), doi: 10.2478/ijame-2022-0055.

[17] M. S. Barak and V. Gupta, 'Memory-dependent and fractional order analysis of the initially stressed piezo-thermoelastic medium', *Mech. Adv. Mater. Struct.*, vol. 0, no. 0, pp. 1–15, May (2023), doi: 10.1080/15376494.2023.2211065.

[18] M. S. Barak, M. Kumari, and M. Kumar, 'Effect of local fluid flow on the propagation of plane waves at an interface of water/double-porosity solid with underlying uniform elastic solid', *Ocean Eng.*, vol. 147, no. May 2017, pp. 195–205 (2018), doi: 10.1016/j.oceaneng.2017.10.030.

[19] A. C. Eringen, 'Linear theory of nonlocal elasticity and dispersion of plane waves', *Int. J. Eng. Sci.*, vol. 10, no. 5, pp. 425–435, May (1972), doi: 10.1016/0020-7225(72)90050-X.

[20] M. A. Ezzat, A. S. El-Karamany, and A. A. El-Bary, 'On dual-phase-lag thermoelasticity theory withmemory-dependent derivative', *Mech. Adv. Mater. Struct.*, vol. 24, no. 11, pp. 908–916 (2017), doi: 10.1080/15376494.2016.1196793.

[21] J. D. Achenbach, *Wave Propagation in Elastic Solids*. Elsevier (1975).

[22] V. Pathania and P. Joshi, 'Waves in thermoelastic solid half-space containing voids with liquid loadings', *ZAMM Zeitschrift fur Angew. Math. und Mech.*, vol. 101, no. 12, pp. 1–19 (2021), doi: 10.1002/zamm.202100093.

[23] D. Singh, D. Kumar, and S. K. Tomar, 'Plane harmonic waves in a thermoelastic solid with double porosity', *Math. Mech. Solids*, vol. 25, no. 4, pp. 869–886 (2020), doi: 10.1177/1081286519890053.

Received June, 2023